E-proceedings of the 38th IAHR World Congress
September 1-6, 2019, Panama City, Panama
doi:10.3850/38WC092019-0409

OPTICAL MEASUREMENT METHOD FOR QUANTIFYING SEDIMENT TRANSPORT IN PHYSICAL EXPERIMENTS

STEFAN SCHÄFER[1], MATHIAS SCHLAGENHAUSER[2] & PETER RUTSCHMANN[3]

[1,2,3] Obernach Hydraulics Laboratory, Technical University of Munich (TUM), Germany
stefan.schaefer@tum.de

[3] Chair of Hydraulic and Water Resources Engineering, Technical University of Munich, Germany

ABSTRACT

The authors present a measurement method that makes it comparatively inexpensive to carry out continuous measurements of sediment transport and display them in real time with very little computing power. The measurement method is part of a system for the continuous diversion or recirculation of sediments discharged from a flume or a laboratory canal. The core of the measurement method is a camera-optical gray value comparison of 8-bit grayscale images of a transparent measuring field, taken with a standard industrial camera. The measuring field consists of two transparent glass plates, one above the other, with a thin film of particle-laden liquid flowing between them (e.g. sand grains or plastic granulate in water). For each image, the concentration of the sediment in the liquid at a discrete point in time is first determined with the help of gray value comparison. The sediment transport $\dot{m}_S$ [kg/s] derives from a calibration function, which was determined in advance from long-term measurements with several constant sediment concentrations. Comparative validation measurements showed measurement errors of around 5 percent for sediment concentrations between 0 and 20 percent.

Keywords: sediment transport; optical measurement; calibration; physical experiments; reservoir management.

1 INTRODUCTION

The quantification of sediment transport is an important task in hydromorphology and of equal importance for geographers, engineers and ecologists. Due to the complexity of sediment transport processes, various forecasting methods have been developed, most of which involve an empirical approach (Yalin, 1972; Zanke, 1982). However, their field of application is mostly limited to specific applications, sometimes only with significant simplifications, so that research on generally valid prediction models is still ongoing (Gyr and Hoyer, 2006; Ancey et al., 2014).

In parallel to theoretical solutions, new measurement methods were continuously developed to quantify sediment transport. In classical methods, which often function very robustly, sediment samples of various sizes are collected over a defined period of time and analyzed later (Van Rijn and Roberti, 2014; Diplas et al., 2008; IAEA, 2005). The greatest weakness of these methods, however, lies in the discontinuous recording of the measurement data. Thanks to great advances in measurement technology and data processing, it has been possible in the recent past to develop non-contact measurement methods with continuous data recording, of which optical and acoustic methods in particular achieve high accuracies (Albayrak et al., 2015; Haimann, 2015; Rüther, 2017; Garcia, 2006).

The range of application of the various measurement methods for hydraulic engineering issues extends from large-scale nature measurements to investigations at grain level and below. At the natural site, the large dimensions of the study area often have a limiting effect, which is why physical laboratory investigations still play an important role in the quantification of sediment transport (Yalin, 1971; Hughes, 1993; Kirkegaard et al., 2011). In the laboratory, complex hydromorphological processes can be simulated under controlled experimental conditions and a large number of different parameters can be recorded simultaneously, reproducibly and with high accuracy.

As part of a research project to investigate sediment transport processes in river reservoirs with predominantly fine sand, a system for the continuous measurement and recycling of solids was developed, which are flushed from the reservoir of a physical laboratory experiment. The discharged solids are collected and fed to a submersible pump, which uses a small proportion of the water flowing through the weir gates to transport the solids back upstream of the reservoir via a pipeline. The measuring field of the optical measuring system presented in this article is integrated into the pipeline and enables continuous measurement of the transport rate. At the same time, the discharged solids can be circulated, which reduces the quantity of solids that would otherwise have to be purchased and stored as supply material for long-term tests without circulation.

At the core of the measurement method is a comparatively simple camera-optical gray value comparison of individual images from a commercially available industrial camera, which depicts the distribution of solid particles (e.g. sand grains or plastic granulate) flowing through a transparent, horizontal measuring field, which is illuminated from below. For each image, the concentration of the solids in the liquid at a discrete point in time is first determined with the aid of the gray value comparison and sediment transport $\dot{m}_s$ [kg/s] is then calculated from the known discharge and the grain density. In contrast to comparable optical methods in which the sediment transport is measured directly in the outlet of the test station (cf. Dhont et al. (2017)), width and flow depth in the test station as well as the amount of mass transported have no direct effect on the quality of the measured values in the measuring field of the measurement method presented.

2 METHODOLOGY

2.1 Optical measuring system

The measuring field consisted of two transparent glass plates arranged horizontally one above the other with a thin sheet of liquid flowing between them. Via a geometric transition element, the liquid flow loaded with solids from the circular pipeline was continuously guided between the glass plates (Figure 1). The transition element was designed to minimize the formation of vortex-inducing flow separation (angle of expansion = 8°, cf. Bollrich (2013)). The sheet between the glass plates was 600 mm x 600 mm in horizontal dimensions and 10 mm high, which was about 2.5 times the height of the largest solid particles to ensure permanent free passage of the measuring field.

The glass plates were illuminated from below so that solid particles created local darkening on their way through the measuring field. An industrial camera was directed at the measuring field from above and depicted the shadows of the solid particles as a gray value image against the otherwise white background. For each pixel of the gray-scale image, the gray-scale value recorded by the camera (8-bit grayscales, value range [0-255]) was compared with a threshold value determined by previous calibration.

Pixels with gray values below the threshold value were assigned the value 0 or white and all others the value 1 or black. In this way, the threshold value comparison transformed the former gray value image into a binary black-and-white image and clearly distinguished for each pixel between the states "black" (= solid particle) and "white" (= no particle). A calibration function was used to assign a solids concentration in the liquid stream to the proportion of black pixels in the overall image.

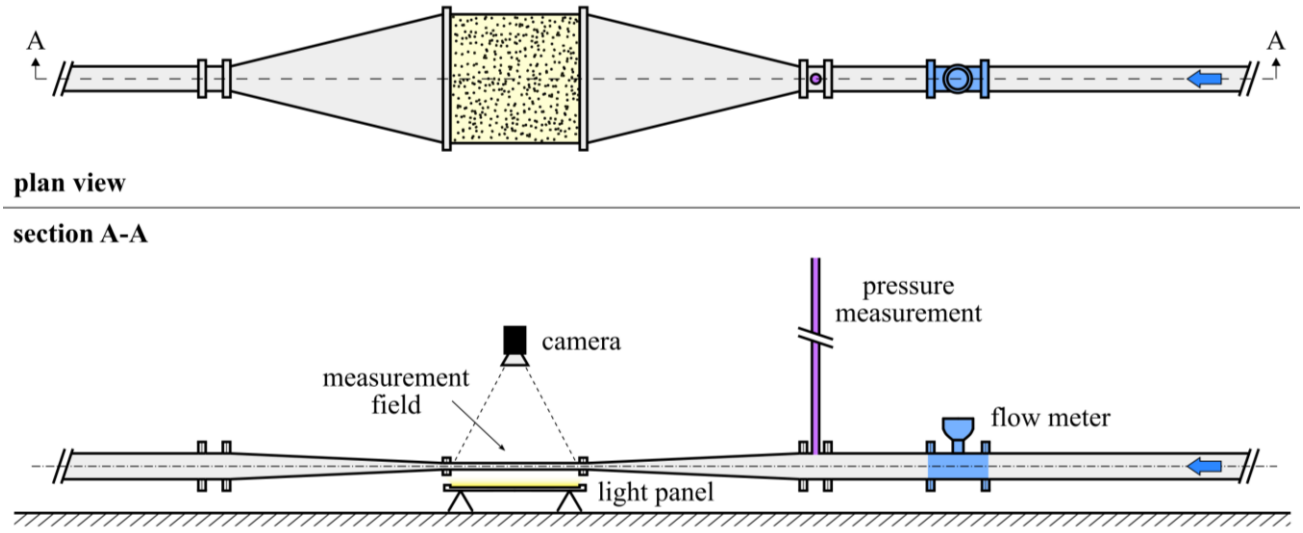

Figure 1. Optical measuring system in plan view and longitudinal section.

2.2 Recirculation system

The optical measuring system was embedded in a system for the continuous recirculation of solids during an experiment. For this purpose, the solids flushed out of the test station were retained in a sediment trap with the aid of an inclined perforated plate. While most of the discharge from the test station flowed through the perforated plate and back into a water reservoir, the solids were collected in a corner of the sediment trap in which there was also the inlet of a dirty water pump (400 V).

This pump had a free passage of grain size up to Ø10 mm and a maximum capacity of 38 l/s in the present study. It was regulated by a frequency converter and it transported the fluid-solid mixture into a pipe with a nominal diameter of 100 mm, in which the discharge was first measured by means of an electromagnetic flowmeter (±0.5 % measurement error (KROHNE Messtechnik GmbH, 2017)). The solid-water mixture flowed past a pressure measurement (±5 mm measurement error) and was then guided into the measuring field of the

optical measuring system. Afterwards, a DN 100 mm pipeline of variable length led towards the beginning of the test station, where the solids were fed back into the reservoir. Therefor diffuser was arranged under water, which evenly distributed the solids over the reservoir width. The flow velocity was over 2 m/s in the entire recirculation system and around 2.8 m/s in the measuring field.

2.3 Calibration system

The calibration function was determined from a large number of long-term measurements with solids concentrations kept constant over the duration of the respective measurement. For this purpose, a smaller part of the recirculation system was operated as a closed circuit, within which the system volume and the volume of the solids added were known (Figure 2).

The supply shaft, which was open at the top, was used to add defined quantities of solids to the circuit and thus gradually increase the solids concentration in the system volume. A water-permeable shut-off membrane just above the pipe axis prevented the presence of solid particles in the supply shaft during operation. The pressure level in the measuring system was also controlled by the water level in the supply shaft. With the help of a small additional flow of water into the supply shaft, its upper edge was always slightly overflowed during operation. The shaft height was fitted in advance to set the desired system pressure.

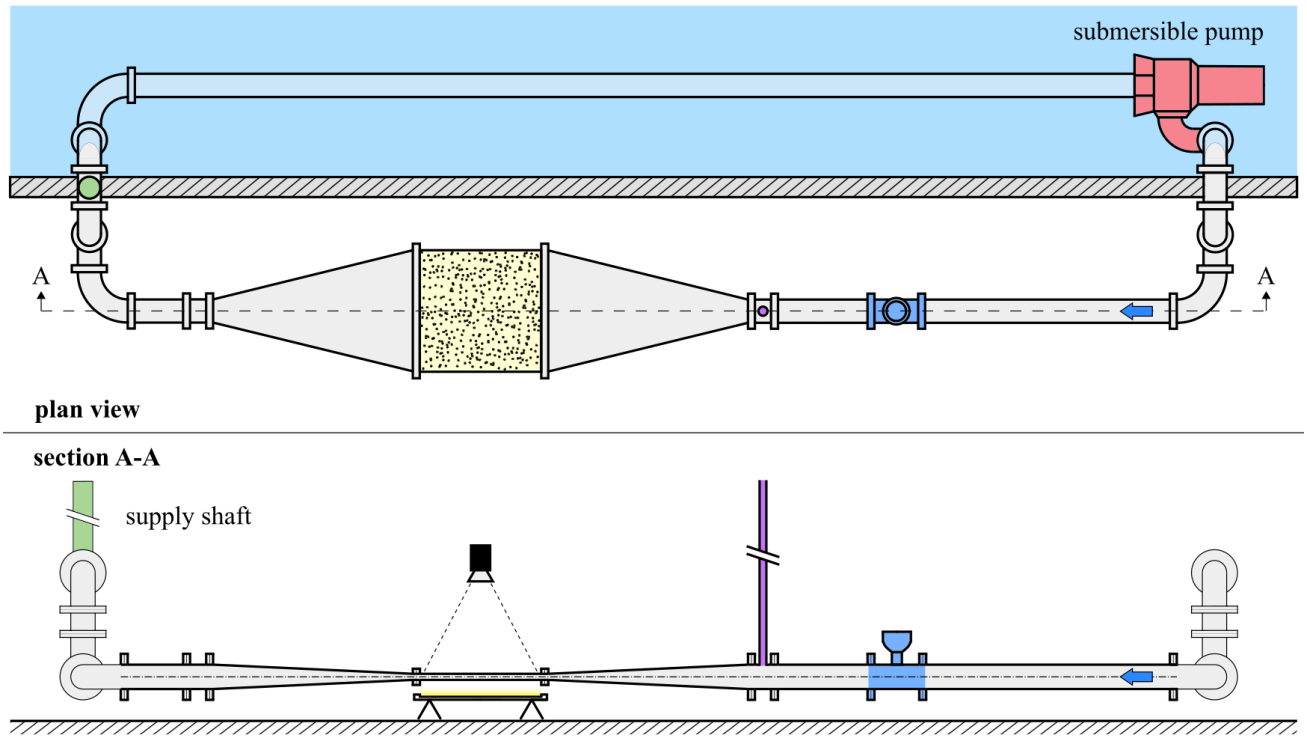

Figure 2. Recirculation system in calibration setup.

3 CALIBRATION OF THE MEASURING SYSTEM

The correlation between gray value and solids concentration was established by calibration measurements. In order to avoid local deposition zones of solids, the greatest possible mixing of solids and liquids had to be ensured during operation. Therefore, flow velocity was chosen so high that the solids were transported at every point with approximately the same velocity as the surrounding liquid. Directional changes in the pipeline course were constructed as streamlined as possible. In this way, systematic errors from the measurement procedure were minimized. Statistical measurement errors, which mainly resulted from turbulent fluctuations in the flow and the statistical distribution of the solid particles in the measuring field, were compensated by long measurement times during calibration.

In the present study, calibration measurements were performed for two uniformly graded lightweight plastic granules with densities of 1.1 and 1.05 g/cm³ and mean grain diameters of 3.7 and 4.1 mm. The calibrated solids concentrations were between 0.5 and 12 % of the system volume. Figure 3 shows the darkening of the measuring field at a concentration of 12 % of the gray granules. Preliminary tests with sand grains were also conducted and showed promising results. However, since sand grains were not used in the physical laboratory experiments that led to the development of the measuring system presented here, no further investigations have been carried out to date.

Several internal and external factors had an influence on the definition of the threshold to distinguish between "particulate" and "no particulate". A gray scale gradient existed from the center to the edge of a solid particle due to scattered light reflected from the side, which was additionally affected by the proportion of fine

air bubbles adhering to the particle surfaces (Raffel, 2007). The identification of the particle edges also depended on externals factors like camera settings (e.g. focal length, aperture) and lighting conditions (e.g. absolute brightness of the light panel and its fluctuations, decrease in brightness from the center to the edge of the lens).

The threshold value below which a gray value was defined to be white and above which it was black had to be set so high that fluctuations in lighting conditions did not directly alter the black-and-white distribution in the binary image. Furthermore, the threshold value had to be set sufficiently high that only those pixels were considered black and thus as particles, which actually represented a solid particle. Pixels that were displayed darker due to lower illumination, i.e. in the edge areas of the measuring field, could not be classified as particles. For this reason, only a square of 1700 x 1700 pixels in the center of the measuring field was analyzed.

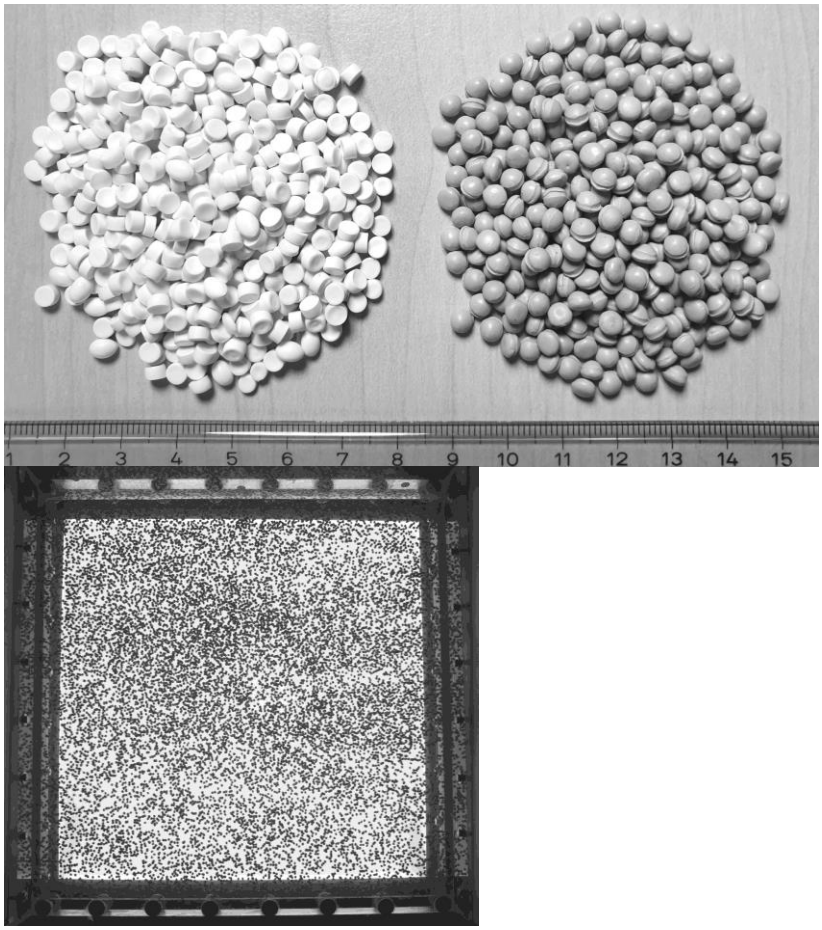

Figure 3. Left: Granules used for calibration. Right: Measuring field during operation (12 % gray granules).

In general, the threshold value should not be set too high because, due to the gray scale difference from the center to the edge of a solid particle, it reduces the black area of a particle and thus the number of black pixels per particle. The lower the proportion of black pixels available for evaluation of the gray value image, the more sensitive the measurement method reacted to concentration fluctuations. For a stable, reliable evaluation process, the highest possible absolute value of pixels evaluated as particles was therefore desirable. All parameters relevant for calibration are presented below.

3.1 Exposure time

For a reproducible approach to image processing, consistently "sharp" images had to be captured. If during the measurements the discharge and thus inevitably the flow velocity had to be varied in order, for example, to increase the transport capacity in the recirculation system for transport peaks with increased pumping performance, a separate calibration function would have to be available for each discharge.

To avoid that, the exposure time would have to be so short during calibration that no relevant movement of the particles would take place within a defined discharge range during exposure. The relevant movement was defined as the proportion of the particle surface at rest that is added by the particle movement during the exposure time and which enlarges the photographed particle surface. The longer the exposure time in relation to the particle motion at a given particle velocity, the more distorted a particle becomes during exposure. Depending on the flow velocity, the same particle would therefore be imaged differently in size or distorted and thus produce a different gray value, which could falsify the measurement result.

In the process described, it is unknown to the authors to what extent an increase in particle area due to particle distortion would lead to an increase in the number of black pixels, and from what point excessive distortion due to residual light would reduce the number of black pixels per particle. This question would have to be verified based on further measurements, which, however, has not been possible with the technical conditions of the measuring system presented so far. For the presented study, the measuring system was therefore operated exclusively with constant discharge.

3.2 Frame rate

Since the analysis of the black-and-white images was done with a statistical approach, the theoretical minimum frame rate depended only on the desired temporal resolution of the concentration variations. However, since perfect mixing could not be guaranteed and the highest possible time resolution was required, the theoretical minimum frame rate in the present study depended on the flow velocity in the measuring field. To ensure continuous measurement, each particle had to be photographed at least once. However, this requirement was not sufficient because a particle at the edge of the image did not provide exactly the same number of black pixels as in the center of the image. Instead, more black pixels tended to be detected for particles closer to the center of the image than for particles at the edge of the image.

Therefore, two images per particle were chosen as the technically reasonable lower limit for the frame rate, so that each particle was recorded at least twice during the passage of the measuring field. Provided that particles in the measuring field were transported exclusively in the direction of flow and without cross-flow components, e.g. by local turbulence, each particle was recorded between the two following edge cases: in the quarter points of the measuring field or centrally and at the edge. On average, there was a balance between a low black pixel value at the edge and a high black pixel value in the center.

3.3 Camera settings

Components with the following specifications were used for the investigations:

- Camera: IDS USB 3 uEye CP 1;
- Sensor: CMOS 2592 x 2048;
- Lens: Kowa f=16mm/F1.4.

The following camera settings were used for the examinations:

- Evaluated pixels: 1700 x 1700;
- Pixel distance in object plane: 0.28 mm;
- Frame rate: 10 Hz;
- Exposure time: 0.3 ms;
- Aperture: F2.0.

3.4 Lens settings

The aperture was chosen relatively wide with F2.0 to collect as much light as possible at a short exposure time. The resulting low depth of field was not a disadvantage for measurement accuracy because the aperture was kept constant for all investigations and was not varied. Particles were almost equally visible along the 1 cm deep liquid film. For practical reasons, the focal length was adjusted to the surface of the upper glass pane of the measuring field. For this purpose, a so-called calibration field with a defined dot grid was fixed to the edge of the upper pane, which was placed on the upper pane before each new measurement in order to check the camera settings. Because the liquid sheet or the actual measuring plane was lower, the particles to be measured were not as sharp as would theoretically have been possible.

This inaccuracy could have been reduced by lowering the camera by the thickness of the glass plate after calibration with the dot grid. In the present study, however, the camera was not repositioned because the camera mount used could not ensure a single vertical movement without influencing the other spatial axes. The influence of the remaining slight uncertainty on the measurement result could not be quantified in the context of the present study. However, given the high accuracy of the validation measurements, these uncertainties were classified as low.

4 OUTCOMES

4.1 Calibration functions

For the two granules used, measurements with constant solids concentrations were carried out step by step. The box plot in Figure 4 shows how the scattering of the measured black pixels per frame increased with increasing solids concentration: higher boxes with 25 and 75% percentiles and longer whiskers with 1.5-fold interquartile distance. The regression line is used to contrast the non-linear relationship between black pixels and solids concentration.

The entire process was repeated several times to evaluate the reproducibility of the calibration functions and it proved to be very good (cf. right side in Figure 4). The confidence limits are close to the regression function derived from the calibration functions. For the slightly less uniformly graded white granulate, both the

distances to the confidence limits were significantly greater and the nonlinearity of the calibration functions more pronounced, which led to a weaker increase in black pixel number with an increase in solids concentration.

4.2 Influence of measurement time

When determining an unknown solids concentration from a single image using the derived calibration function, the resulting measurement error was dependent on the random fluctuation of the recorded black pixel values. In order to quantify this error, the temporal development of the mean values was examined. The left side of Figure 5 shows the temporal development of the mean values at constant solids concentrations during calibration. At the latest after five seconds all mean values were approximately constant.

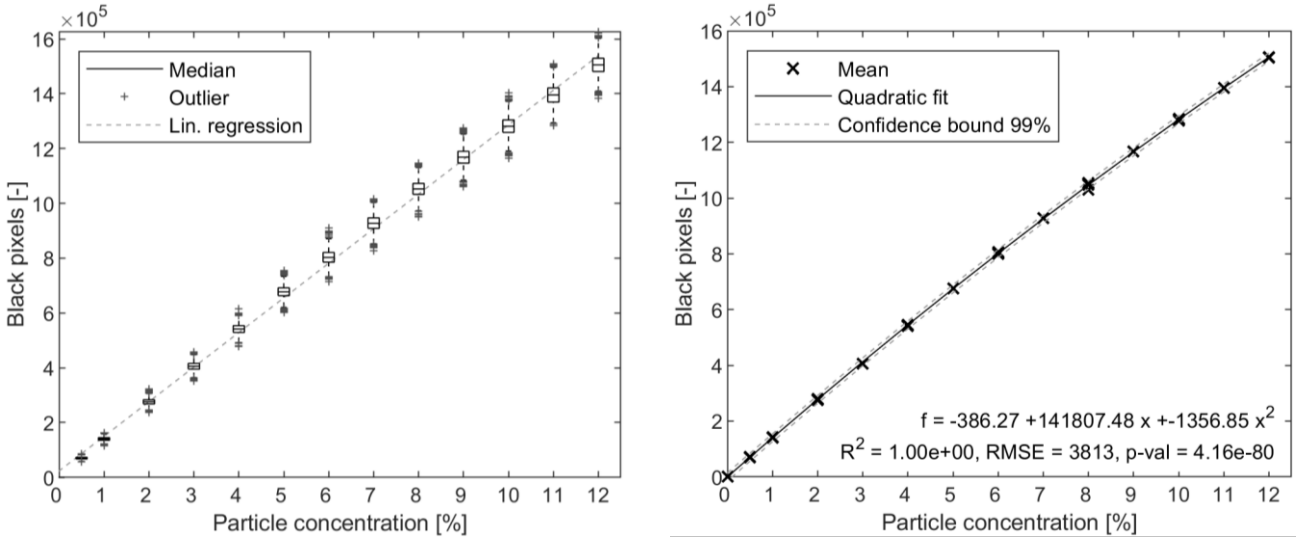

Figure 4. Results of calibration measurements for the gray granules. Left: Box plot of one calibration run. Right: Regression of four calibration runs.

However, this information involves a certain amount of uncertainty because of the fluctuations in the measured values. In order to derive a reliable averaging time, the normalized mean squared error (NMSE), which was defined by González-Castro, et al. (2000) as follows, was also evaluated:

$$\mathrm{NMSE} = \frac{\overline{(\mathrm{P_T} - \mathrm{P})^2}}{\overline{\mathrm{p'^2}}} \qquad [1]$$

with

P … Average black pixel value of a long-term measurement [-];

$\mathrm{P_T}$ … Average black pixel value of a time series of length T [-];

$\overline{\mathrm{p'^2}}$… Variance of black pixel values of a long-term measurement [-].

The NMSE is used to evaluate the required measurement time with regard to the temporal randomness of a single measurement. The NMSE normalizes the mean squared error (MSE) using the variance of a data set (here: black pixel values of a long-term measurement) and gives the deviation of the mean value after a certain measurement time from the long-term mean value. Compared to the left side, the right side of Figure 5 shows clear differences between the individual time series, which also show no proportionality to the solids concentration.

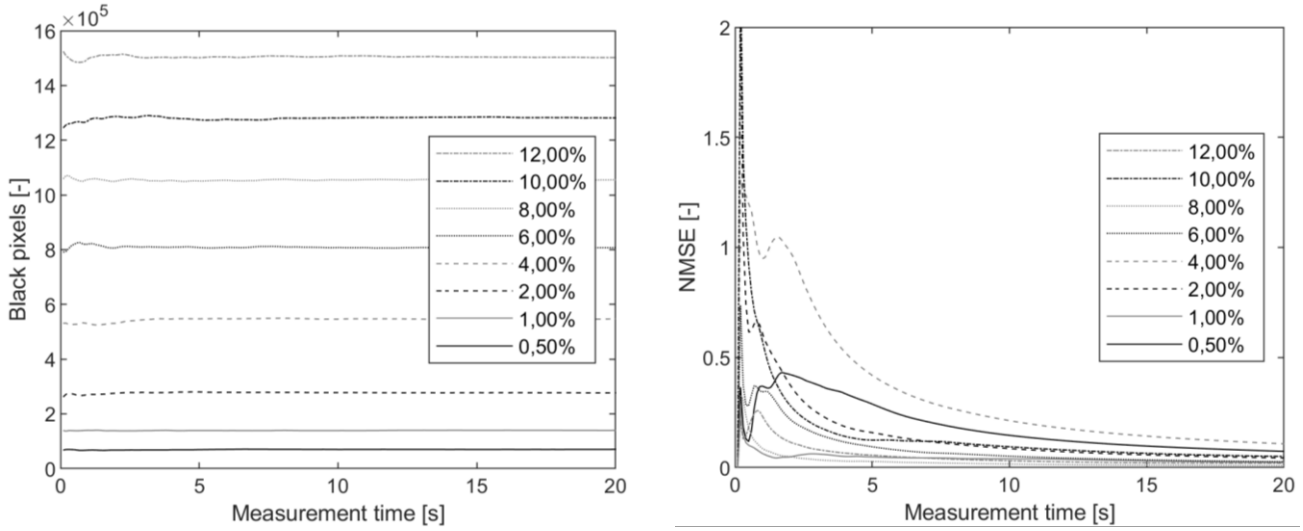

Figure 5. Temporal development of statistical parameters for the gray granules. Left: Mean value development for one calibration run. Right: Corresponding NMSE development.

With a desired NMSE ≤ 20%, 10 s were chosen as the minimum required averaging time. The temporal resolution of the measurement method was directly affected by this. Transport processes that took place in shorter time periods could not be recorded with the presented boundary conditions.

4.3 Validation measurements

The accuracy of the derived calibration function was checked by means of validation measurements. For this purpose, defined quantities of solids were fed directly into the inlet of the recirculation system and recorded via the measuring field. Figure 6 shows the measured values recorded at 10 Hz in light gray and a notably simplified data curve of stepwise averaged values with an averaging interval of 10 s in black, where the whole data set was partitioned in steps of the averaging interval. In the given example, each averaging interval had 100 values (10 Hz * 10 s), which explains the jagged curve. For comparison, a moving average curve is given as a dashed line, also with a window length of 10 s, which is smoother due to the larger amount of data points, but which lags in time due to the relatively long averaging interval.

Of the 49.5 kg added in a short time, only 47.3 kg were recorded, which corresponds to an absolute measurement error of < 5%. After subtracting a minor loss during addition, the high peak load is particularly responsible for the measurement error. The solids concentration at the peak was about 17%, which was significantly above the secured calibrated range (12 %). In addition, the peak duration was less than three seconds and thus significantly shorter than the minimum required averaging time. Based on comparable data sets, the calibration function could be extrapolated to cover even higher concentrations. Comparative tests with solids concentrations up to 20% showed good results, but since such peaks did not occur during the operation of the test station in the present study, no additional validation measurements were required.

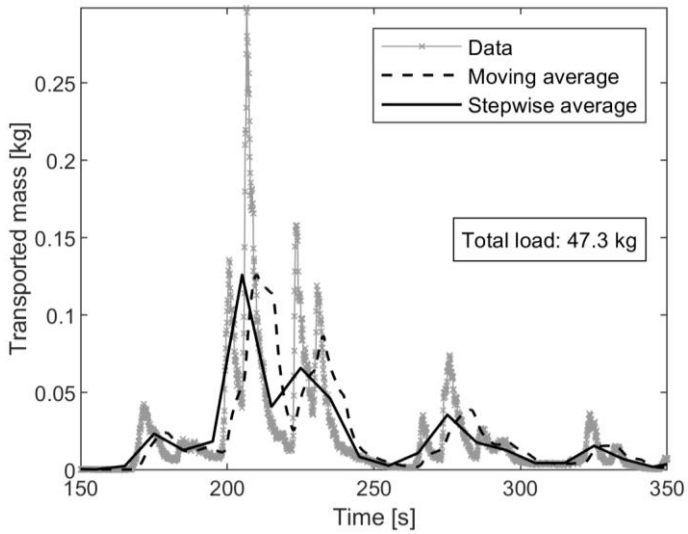

Figure 6. Validation time series with stepwise and moving average of a 49.5 kg sample.

During experiments, the measuring system was operated for many hours without any problems. In experiments with increased sediment transport, up to 10 t of material were transported through the recirculation system and measured. With an experiment duration of 8 hours, this corresponds to an average transport rate of 0.35 kg/s.

5 DISCUSSION

5.1 Uncertainties in the measurement procedure

Solids composition: Depending on the composition of the solids used, the particle sizes and shapes vary, and as a result the measurement uncertainty changes. In the simplest or statistically most reliable case, a single-grain material with perfectly spherical particles, the gray value of two camera images varies only due to the different particle distribution in the measuring field. In the case of solids with less uniform particle distributions and non-spherical particles, the formation of shadow, which is variable due to the orientation and size of the particles, is added as a variable for the proportion of black pixels in the single image. Due to a high variability of the particle geometry of the solids, the statistical uncertainty of a single measurement increases, which could however be compensated by a higher frame rate. An increase in the frame rate generally reduced the statistical uncertainty from the particle geometry and orientation and it is a useful measure with increasing heterogeneity of the solids, as long as no relevant quality losses of the individual images have to be accepted.

Flow conditions: If one could assume perfect mixing of the fluid-solid mixture and assume an equal distribution of the particles in the fluid at all times, a much lower frame rate would also be sufficient to determine the transport rate. In the present study, however, the solid particles used were relatively large and the volume considered rather small, which led to a high variability of the black pixel number in the measuring field. Furthermore, the particle load of the submersible pump was not constant, which is why the assumption of perfect mixing could not be made. Nevertheless, the mean values became stable within a very short period of time (cf. Figure 5, right). Furthermore, parameters assumed to be constant, such as pump performance, fluctuate and have a direct effect on the measurement result.

System pressure: The system pressure, or more precisely the static pressure level in the measuring field, also had a significant influence on the measurement results. Fluctuations in the static pressure level led to proportionally fluctuating black pixel numbers at constant solids concentrations, even if all other parameters remained constant. The pressure height was regulated by means of a vertical shaft integrated into the recirculation system, originally to dampen fluctuations in pump performance, and subsequently kept constant for all measurements. The following two mechanisms probably played a role here: On the one hand, fine gas bubbles were found on the particle surfaces, which changed their size depending on the system pressure and thus also influenced the scattering of the light coming from the light panel under the measuring field. On the other hand, a slight curvature of the glass plates of the measuring field to the outside, depending on the system pressure, could not be excluded, whereby particles would flow past the camera at a slightly smaller distance than calibrated. However, neither of these mechanisms could be demonstrated in the present study, which is why a final explanation of this phenomenon is still pending.

Camera position: The size of the projected particle surface, that was identified as black by the threshold, varied along the measuring field. The following reasons were identified: A particle in the center of the image was displayed sharper than at the edge of the image, i.e. with a greater gray value gradient at the particle edges, because hardly any scattered light brightened the particle edge due to the vertically incident light rays. A particle at the edge of the image, on the other hand, reflected parts of the light coming from below to the side in the direction of the camera, making the particle edge in this area brighter. Depending on the intensity of the scattered light, pixels in the edge area fell below the threshold for distinguishing between white and black, reducing the particle area imaged as black. In addition, the greater distance of a particle at the edge played a role, because particles further away from the camera occupied fewer pixels, i.e. were imaged smaller. The change of the particle surface was not ideally linear-radial from the center to the edge, but was significantly influenced by the structure of the optical system as well as the installation and alignment of camera and measuring field to each other. For this reason, the camera was permanently installed and fixed so that the height above the measuring field could be reproducibly adjusted and kept constant. The same applied to the orientation of the camera in space.

5.2 Advantages and disadvantages in comparison to other methods

The measurement method is not dependent on the dimensions and transport conditions of the test station, which is why either bed load transport or total transport can be measured. A large spectrum of solids can be measured as long as the solid particles are still large or heavy enough that they can be separated from the surrounding water in the sediment trap. Due to the very small data volume, there is practically no limit to the measurement duration.

Disadvantages of the measurement method are the increased effort involved in preparing and performing the calibration measurements. In addition, there is only little flexibility to making adjustments to the measuring system. A certain calibration function can only be exact if all parameters set during calibration are also set the

same during measurement. A change in the discharge in the measuring system would change the relationship between black pixels and solids concentration even if all other parameters were kept constant.

This low flexibility in operation could be improved by a different evaluation method of the camera images, e.g. particle detection. However, particle superposition in the measuring field would lead to measurement errors in a method with particle detection if the transport rate were determined there via the measured number of solid particles. Reducing the height of the liquid sheet in the measuring field to only slightly more than the diameter of a single particle would largely prevent the occurrence of particle overlaps. In these conditions, particle detection would present an alternative to calibrated gray value comparison and the time-consuming calibration measurements would no longer be necessary. In preliminary investigations, however, such a reduction led to the successive blockage of the measuring field and proved to be impracticable.

6 CONCLUSION

The presented measurement method is able to generate high-quality information about the transport of solids during experiment operation in real-time and with very low computing power. The required calibration proved an efficient way to reduce systematic uncertainties in the measurement procedure by implicitly taking them into account in the calibration function. The measurement accuracy achieved in the thin liquid sheet is comparatively high with around 5% and below, while at the same time a wide range of particle loads can be measured (0 - 20%). With further research effort, the remaining uncertainties could be quantified more precisely, which could potentially increase the measurement accuracy even more. Integrating the measurement method into a system for the recirculation of solids can bring financial benefits especially for long-term experiments, since hardly any additional supply material is required.

REFERENCES

Albayrak, I., Felix, D., Hagmann, M., Boes, R.M., 2015. Suspended Sediment and Bed Load Transport Monitoring Techniques, in: Dresdner Wasserbauliche Mitteilungen Heft 53. Presented at the 38. Dresdner Wasserbaukolloquium 2015, Technische Universität Dresden, Institut für Wasserbau und Technische Hydromechanik.

Ancey, C., Bohorquez, P., Bardou, E., 2014. Sediment transport in mountain rivers. ERCOFTAC Bulletin 100, 37–52.

Bartram, J., Ballance, R., United Nations, World Health Organization (Eds.), 1996. Water quality monitoring: a practical guide to the design and implementation of freshwater quality studies and monitoring programmes, 1st ed. ed. E & FN Spon, London ; New York.

Bekić, D., Mikoš, M., Babić-Mladenović, M., Kupusović, T., Oskoruš, D., 2015. Review of technical international standards and techniques for sediment monitoring, in: Towards Practical Guidance for Sustainable Sediment Management (SSM) Using the Sava River Basin as a Showcase. Presented at the Workshop on sediment monitoring, Zagreb.

Bollrich, G., 2013. Technische Hydromechanik 1: Grundlagen, 7th ed. Beuth.

Dhont Blaise, Rousseau Gauthier, Ancey Christophe, 2017. Continuous Monitoring of Bed-Load Transport in a Laboratory Flume Using an Impact Sensor. Journal of Hydraulic Engineering 143.

Diplas, P., Kuhnle, R., Gray, J., Glysson, D., Edwards, T., 2008. Sediment transport measurements: Chapter 5, in: Marcelo H. García (Ed.), Sedimentation Engineering: Processes, Measurements, Modeling, and Practice. American Society of Civil Engineers, pp. 307–353.

García, M.H., 2006. ASCE Manual of Practice 110 - Sedimentation Engineering: Processes, Measurements, Modeling and Practice, in: World Environmental and Water Resource Congress 2006.

González-Castro, J.A., Oberg, K., Duncker, J.J., 2000. Effect of Temporal Resolution on the Accuracy of ADCP Measurements, in: Joint Conference on Water Resource Engineering and Water Resources Planning. American Society of Civil Engineers, Minneapolis, Minnesota.

Gyr, A., Hoyer, K., 2006. Sediment Transport: A Geophysical Phenomenon, 2006 edition. ed. Springer, Berlin etc.

Haimann, M., 2015. Sediment Transport Monitoring and Modelling, in: Towards Practical Guidance for Sustainable Sediment Management (SSM) Using the Sava River Basin as a Showcase. Presented at the Workshop on sediment monitoring, Zagreb.

Hughes, S.A., 1993. Physical models and laboratory techniques in coastal engineering, Advanced series on ocean engineering. World Scientific, Singapore.

International Atomic Energy Agency (IAEA), 2005. Fluvial sediment transport: analytical techniques for measuring sediment load. International Atomic Energy Agency, Vienna.

Kirkegaard, J., Wolters, G., Suterhland, J., Soulsby, R., Frostick, L., McLelland, S., Mercer, T., Gerritsen, H., 2011. Users guide to physical modelling and experimentation, 1. ed., IAHR design manual. CRC Press, Boca Raton etc.

KROHNE Messtechnik GmbH, 2017. OPTIFLUX 2000 - Technical Datasheet. Duisburg.

Raffel, M., 2007. Particle image velocimetry: a practical guide. Springer, Berlin.

Rüther, N., 2017. State of the art of sediment transport measurement techniques in rivers and reservoirs. [WWW Document]. URL http://folk.ntnu.no/nruther/TVM4155/Lecture14-NR/Sediment%20transport%20measurement%20techniques.pdf (accessed 4.5.19).

Van Rijn, L.C., Roberti, H., 2014. Manual Sediment Transport Measurements in Rivers, Estuaries and Coastal Seas - Coastal Wiki [WWW Document]. URL http://www.coastalwiki.org/wiki/Manual_Sediment_Transport_Measurements_in_Rivers,_Estuaries_and_Coastal_Seas#cite_ref-1 (accessed 4.5.19).

Yalin, M.S., 1972. Mechanics of sediment transport. Pergamon Press, Oxford; New York.

Yalin, M.S., 1971. Theory of Hydraulic Models. Macmillan Education, Limited, London.

Zanke, U., 1982. Grundlagen der Sedimentbewegung. Springer, Berlin; New York.